Diagenetic Mg-calcite overgrowths on foraminiferal tests in the vicinity of methane seeps

Giuliana Panieri[1*], Aivo Lepland [1,2,3,4], Martin J. Whitehouse[5], Richard Wirth[6], Morten P. Raanes[7], Rachael H. James[8], Carolyn A. Graves[9], Antoine Crémière [1,2], Andrea Schneider[1]

[1]CAGE - Center for Arctic Gas Hydrate, Environment and Climate, Department of Geology, UiT University of Norway, Tromsø, Norway. E-mail: giuliana.panieri@uit.no

[2]Geological Survey of Norway, 7491 Trondheim, Norway

[3]Institute of Geology, Tallinn University of Technology, 19086 Tallinn, Estonia

[4]Department of Geology, University of Tartu, Ravila 14A, 50411Tartu, Estonia

[5]Department of Geosciences, Swedish Museum of Natural History, PO Box 50 007, SE-10405 Stockholm, Sweden

[6]GeoForschungsZentrum Potsdam, Telegrafenberg, Chemistry and Physics of Earth Materials, D-14473 Potsdam, Germany

[7]Department of Materials Science and Engineering, Norwegian University of Science and Technology, 7491 Trondheim, Norway

[8]Ocean and Earth Sciences, National Oceanography Centre Southampton, University of Southampton, Southampton SO14 3ZH, UK

[9]Leibniz-Institute for Baltic Sea Research, Rostock, Germany

** corresponding author*

ABSTRACT

Methane is a potent greenhouse gas and some episodes of past global warming appear to coincide with its massive release from seafloor sediments as suggested by carbon isotope records of foraminifera. Here, we present structural, geochemical, and stable carbon isotope data from single foraminiferal calcite tests and authigenic Mg-calcite overgrowths in a sediment core recovered from an area of active methane seepage in western Svalbard at ca. 340 m water depth. The foraminifera are from intervals in the core where conventional bulk foraminiferal $\delta^{13}C$ values are as low as -11.3 ‰. Mg/Ca analyses of the foraminiferal tests reveal that even tests for which there is no morphological evidence for secondary authigenic carbonate can contain Mg-rich interlayers with Mg/Ca up to 220 mmol/mol. Transmission electron microscopy (TEM) of the contact point between the biogenic calcite and authigenic Mg-calcite layers shows that the two phases are structurally indistinguishable and they have the same crystallographic orientation. Secondary ion mass spectrometry (SIMS) analyses reveal that the Mg-rich layers are strongly depleted in ^{13}C ($\delta^{13}C$ as low as -34.1 ‰). These very low $\delta^{13}C$ values indicate that the authigenic Mg-calcite precipitated from pore waters containing methane-derived dissolved inorganic carbon at the depth of the sulfate-methane transition zone (SMTZ). As the depth of the SMTZ can be located tens of metres below the sediment-seawater interface, interpretation of low foraminiferal $\delta^{13}C$ values in ancient sediments in terms of the history of methane seepage at the seafloor must be undertaken with care.

1. Introduction

Since the discovery of methane emissions at the seabed, investigators have explored the potential of using tests of modern and fossil calcitic foraminifera as archives of seepage history. Remarkable carbon isotope excursions (CIE), characterized by very low $\delta^{13}C$ values in both benthic and planktonic foraminiferal calcite, have been interpreted to reflect widespread release of isotopically-light carbon from dissociating marine methane hydrates during the Paleocene-Eocene Thermal Maximum (PETM) at ~54.95 Ma (e.g., Dickens et al. 1995, Zachos et al. 2005). Massive methane releases have been also used to explain CIEs at other time intervals related to abrupt global warming (Hesselbo et al., 2000, Jiang et al. 2003). However, it remains unclear if the very low $\delta^{13}C$ values of foraminifera reflect δ^{13}C values of dissolved inorganic carbon (DIC) in the primary biomineralization environment or whether they are associated with secondary overgrowths of authigenic carbonate. Very low δ^{13}C values in foraminiferal calcite are widely considered to reflect seepage and incorporation of methane-derived, ^{13}C-depleted DIC at the time when foraminifera calcify their tests (Wefer et al., 1994; Dickens et al., 1995; Kennett et al., 2000; Hill et al., 2004). Alternatively, low foraminiferal δ^{13}C values may reflect precipitation of secondary overgrowths of methane-derived authigenic carbonates forming at the sulfate-methane transition zone (SMTZ) within subsurface sediments (Torres et al., 2010; Millo et al., 2005; Martin et al., 2010; Panieri et al. 2014, 2015; Consolaro et al., 2014). In this scenario, the original test surface merely acts as a template for authigenic carbonate precipitation. At the depth of the SMTZ, upward migrating methane and downward diffusing sulfate are consumed, by anaerobic oxidation of methane (AOM), according to the reaction (Boetius, 2000):

$$CH_4 + SO_4^{2-} \longrightarrow HCO_3^- + \ HS^- + H_2O$$

The bicarbonate (HCO_3^-) ions produced by AOM react with calcium and magnesium ions present in sediment pore waters to form Ca-Mg carbonates (Berner, 1970; Jørgensen et al., 2004; Ussler III and Paull, 2008) which are typically strongly ^{13}C depleted.

Methane-derived authigenic calcite occurring as sediment cements or as overgrowths on foraminifera tests are commonly rich in Mg with Mg/Ca often >20 mmol/mol. Mg is effectively complexed by sulfate in normal seawater which inhibits Mg incorporation into calcite, but if sulfate concentrations are very low, e.g. in pore waters affected by AOM, Mg is not complexed and can be more readily incorporated in calcite (Walter, 1986; Wright and Wacey, 2004). Hence Mg enrichment observed in foraminiferal tests can be indicative of the presence of diagenetic phases.

Here we present the results of analyses of individual foraminifera tests in a sediment core from an area of methane seepage west of Prins Karls Forland (ca. 340 m water depth), offshore western

Svalbard (Fig. 1). Scanning Electron Microscope Energy Dispersive X-ray Spectroscopy (SEM-EDS), Electron Probe Micro Analysis (EPMA), Transmission Electron Microscopy (TEM), and Secondary Ion Mass Spectrometry (SIMS) studies reveal that there is significant variation in the geochemical and carbon isotope compositions *within* individual tests, and highlight the complexity of distinguishing primary vs. secondary signals. We demonstrate that diagenetic overprints on foraminifera can be very extensive, but not always evident using traditional methods such as optical microscopy and SEM.

2. Material selection

Foraminiferal tests were picked from three intervals (core depths 102, 132 and 210 cm below seafloor (bsf); Table 1) within a 224 cm long sediment core PC06 (78:36.66 N; 9:25.53E; 374 m water depth) collected during RRS James Clark Ross cruise 253 in August 2011 (Fig. 1). The present-day depth of the SMTZ in this core is 184 cm bsf, and all sediments from between 100 and 220 cm bsf contain foraminifera with distinctly negative bulk δ^{13}C values (Panieri et al., 2016), outside of the range of normal marine values (ca. -1 to 1 ‰). From each of the three selected intervals calcitic tests of two benthic species, *Nonionella labradorica* (Dawson, 1860) and *Melonis barleeanus* (Williamson, 1858), were chosen for detailed study to assess whether the low δ^{13}C values (Table 1) are associated with primary biogenic calcite, or secondary overgrowths.

3. Strategy

Sediment samples were washed through a 63 μm sieve, and oven dried at 40 °C. Tests of calcitic benthic foraminifera, including both well preserved and altered (with obvious dissolution features and overgrowths) specimens, were picked from the larger size fraction, >100 μm, under a light microscope. The selected specimens (F1-F5) are listed in Table 2, together with results of analysis of the carbon isotope composition of bulk foraminifera (Panieri et al., 2016).

3.1 Scanning Electron Microscope equipped with Energy Dispersive X-ray Spectroscopy (SEM-EDS)

Polished cross-sections of a selection of tests were made by (i) placing the hand-picked tests on adhesive tape in a circular 25 mm diameter mold, (ii) mounting using Struers Epofix, and (iii) polishing to expose a cross-section through the interior of the tests. SEM-EDS examination of these polished sections was carried out at The Arctic University of Norway using a SEM Hitachi Tabletop Microscope TM-3000 equipped with Bruker Quantax 70 EDS Detector, and on a Zeiss Merlin Compact VP with the GEMINI I electron column, and a Zeiss Sigma.

3.2 Electron Probe Micro Analysis (EPMA)

Quantitative Mg and Ca spot analyses and semi-quantitative elemental mapping were carried out using a JEOL JXA-8500F electron microprobe (field-emission electron gun) equipped with a high resolution wavelength X-ray dispersive spectrometer (WDS) at the Department of Materials Science and Engineering in Trondheim. Diopside $MgCaSi_2O_6$ (Mg = 11.23 wt%) and Calcite $CaCO_3$ (Ca = 39.98 wt%) were used as standards. The mapping was performed using a 0.1 µm step size and beam scan with an image resolution of 512 x 512 pixels, 10 kV accelerating voltage and an electron beam current of 20nA with a minimum probe size of 50nm. Under such microprobe conditions the electron diffusion region of X-ray generation is in the range of 1µm (X-ray spatial resolution during mapping). Optimum quantitative counting strategies from Mg and Ca were obtained with a total counting time of 60 seconds in both peak and background position, from an excitation cross-section of approx. 2µm. The reproducibility of Mg and Ca determined from repeated analysis of standards was <1.5 %, and the detection limit was ~100 ppm. Raw data were reduced to weight percentages using the ZAF algorithm. Performing WDS on carbonate material can result in beam damage to the specimen and lower counts compared to materials such as silicates. However, the ratio of Mg to Ca is not severely affected by these effects. Topographic variations and impurities within the foraminifera tests such as clay particles and organic matter can influence the quantification of Mg and Ca in carbonate by EPMA. To minimize these effects, the specimens were carefully examined by SEM- BSD/EDS, and areas that appeared to be impurity-free were selected for EPMA.

3.3 Transmission Electron Microscopy (TEM)

Focused ion beam (FIB) milling was used as a sample preparation method for measurements by transmission electron microscopy (TEM). FIB was conducted on a C-coated polished mount to extract two foils from a single foraminifera test using a FEI FIB2000-TEM equipped with a Ga-ion source at GeoForschungsZentrum Potsdam (GFZ; Germany). FIB milling occurred at 30 keV. Final polishing of the surface with the ion beam almost parallel the surface occurred at a beam current 11 pA. This leads to minimal damage to the outer layer (10 - 15 nm) and, as the thickness of the foil is ~150 nm, the crystalline state of the carbonate that is documented in electron diffraction and lattice fringes, is unaffected. The experience of having cut more than 5000 foils from different materials including many carbonates guarantees that a complete amorphisation of the carbonates by Ga ion sputtering is excluded. The FIB-foil dimension was 15 x 10 x 0.15 μm on average. Milled FIB foils were lifted out of the FIB sputtering site and subsequently placed on standard Cu TEM grids covered with perforated amorphous carbon film (Wirth, 2009). The TEM at GFZ used for this study was a FEI TecnaiG2 F20 X-TWIN equipped with a Gatan Imaging Filter GIF (Gatan Tridiem, Gatan, CA, USA) EDAX X-ray analyzer and a Fishione high-angle annular dark-field detector (HAADF). The electron source of the TEM was a field emission gun emitter, operated at an acceleration voltage of 200 kV. EDX analyses were performed in scanning transmission mode (STEM) by scanning the electron beam within a preselected area. This technique minimizes mass-loss caused by electron sputtering.

3.4 Carbon isotope analyses by secondary ion mass spectrometry (SIMS)

High spatial resolution carbon isotope analyses (c. 15 µm analytical spots) were performed on two mounted foraminifera tests using a CAMECA IMS 1280 large geometry Secondary Ion Mass Spectrometry (SIMS) at the NordSIM facility in Stockholm, Sweden. A critically focused Cs^+ primary beam with 20 keV impact was used to sputter the sample, and a low-energy electron-flooding gun was used for charge compensation. The primary beam current was ca. 3 nA. Each analysis consisted of an initial pre-sputter over a rastered 20 µm area to remove the gold coating, followed by centering of the secondary beam in the field aperture (field of view on the sample of 30 µm with 90x magnification transmission ion optics). Secondary ion signals were measured in multicollector mode using a Faraday detector for $^{12}C^-$ (ca. 2×10^7 cps), and an ion counting electron multiplier for $^{13}C^-$ at a mass resolution of ca. 4000, sufficient to resolve ^{13}C from $^{12}C^1H$. A within run correction was made for electron multiplier gain drift using the pulse height analysis curve. The secondary magnet field was locked at high stability using a nuclear magnetic resonance field sensor operating in regulation mode. All pre-sputter, beam centering and data acquisition steps were automated in the run definition. Typical internal precision obtained for individual run $^{13}C/^{12}C$ ratios from twenty-four cycles of 4-second integrations was ca. 0.2 ‰ (SE). Sample chamber vacuum was maintained at $<2 \times 10^{-8}$ mbar.

Fully automated sequences comprised two measurements of the reference carbonate, Brown Yule Marble calcite (BYM, $\delta^{13}C$ VPDB = -2.28 ‰, kindly provided by J. Craven, University of Edinburgh), bracketing six measurements of unknown targets of the foraminiferal calcite and authigenic Mg-calcite. Calcite and Mg-calcite can be expected to display different instrumental mass fractionation (IMF) during SIMS analysis, hence using the same calcite reference material for foraminiferal calcite and authigenic Mg-calcite may not be fully appropriate. An IMF bias between calcite and various Mg-containing carbonates has been demonstrated for oxygen isotopes (Rollion-Bard & Marin-Carbonne, 2011) and measurements of carbon isotopes in dolomite and calcite reference materials at NordSIMS have yielded a bias of -0.33‰ per wt. % of MgO (MJW unpublished data), similar to the reported bias for oxygen. This implies that Mg-calcite with Mg/Ca of 220 mmol/mol normalized against calcite will be approximately 2‰ too light. Assuming a similar linearity in the IMF bias for carbon as has been demonstrated for oxygen, the effect will be proportionally smaller at lower Mg abundance. The putative instrumental mass bias effect thus has a relatively minor influence on the acquired isotope ratios and, given the much greater magnitude of the observed differences, does not affect our interpretations. The regularly interspersed BYM measurements were used to correct measured isotope ratios for any drift during the analytical session (typically a cubic polynomial fit was made to the standard analyses) and for instrumental mass fractionation (IMF). External precision on δ^{13}C based on multiple analyses of the BYM standard was <0.4 ‰ (SD). Carbon isotope compositions are reported in conventional δ notation relative to Vienna PeeDee Belemnite (VPDB).

4. Results and discussion

4.1 SEM evidence for the presence of [cryptic] authigenic carbonate

SEM analyses reveal the presence of abundant diagenetic pyrite and authigenic carbonate on the foraminiferal test walls (Fig. 2). Co-precipitation of these phases can be expected at the depth of the SMTZ, because AOM results in the production of bicarbonate and hydrogen sulfide, which induces precipitation of authigenic carbonate minerals and pyrite (Peckmann et al., 2001). These authigenic carbonate overgrowths can be ‘cryptic’, i.e. they are not visible under optical microscope. For instance, relatively well preserved tests with typical granular microstructure and wall pores and no obvious evidence for authigenic carbonate overgrowths, contain clusters of framboidal pyrite inside the test chambers (Fig. 2a-b). The extent of authigenic carbonate overgrowths can be highly variable both between and within individual tests. In sediments from 132 cm bsf, tests without obvious overgrowths (Fig 2a) and tests with thick overgrowths (Fig. 2h) co-occur. In some tests there is a gradient from thick overgrowths on the test walls of the outer chambers to thin overgrowths on the test walls of the inner chambers in the umbilical region (Fig. 2c). The pores appear to act as a nuclei for precipitation of authigenic carbonate, as suggested by linings of authigenic crystals around the pores in the inner chambers (Fig. 2d). The outer chambers are variably covered with the overgrowths; authigenic carbonate precipitation takes place in spaces between the pores (Fig. 2e) and eventually the whole inner side of the test can become covered with microcrystalline overgrowths completely masking the original surface features of calcite tests (Fig. 2f-h).

4.2 Mg/Ca in biogenic calcite and authigenic carbonate overgrowths

Morphological evidence for authigenic carbonate overgrowths on the tests from core PC06 is supported by differences in the Mg/Ca ratio of the original test calcite and the overgrowths. EBS images and EPMA Mg/Ca mapping show the presence of low EBS and relatively Mg-rich overgrowths approximately 20 μm thick, on both the inner and outer foraminiferal test walls (Fig. 3). The Mg/Ca ratio of the overgrowths is as high as 220 mmol/mol, while the Mg/Ca ratio of the original test calcite is < 10 mmol/mol. The occurrence of Mg-rich authigenic phases is not however limited to the overgrowths on test walls; these authigenic phases can also fill the original wall porosity and pores within it.

Some specimens are compositionally laminated with distinct Mg-rich laminae (Fig. 3). The initial lamination was likely formed during ontogenesis as calcite laminae are added to the pre-existing test every time a new chamber is built. Calcite crystallites in such laminae have a radial appearance with C-axes lying perpendicular to the lamination, facilitating high porosity (Erez, 2003). Organic material deposited between the calcite laminae can also become porous upon mineralization of organic matter resulting in porous laminae. These pores are likely susceptible to filling by authigenic Mg-rich calcite during diagenesis. The result is a systematic banding with alternating high and low Mg/Ca.

Quantitative EPMA point analyses (ca. 2 µm diameter spot) show that Mg/Ca in Mg-rich zones ranges from 10-60 mmol/mol in thin interlayers and in-filled pores while thicker overgrowths can have Mg/Ca up to 220 mmol/mol (Table 3, Fig. 4). Given that the thin Mg-rich layers and pores are commonly smaller than the analytical spot size of the EPMA, the measured Mg/Ca ratios of the authigenic carbonates are likely lower than the actual Mg/Ca ratios due to contributions from enclosing low-Mg phases. The Mg/Ca ratio of foraminiferal calcite is a widely accepted and applied proxy for ocean temperature (Bohaty et al., 2012; Elderfield and Ganssen, 2000; Garidel-Thoron et al., 2005; Lea et al., 2000; Nürnberg et al., 2000), and variable Mg/Ca with distinct banding or apparently random variations in calcite tests can be produced by temperature variations during foraminiferal growth (Sadekov et al., 2005; Branson et al., 2013). However, these variations are typically in the range 2-10 mmol/mol. Given that Mg/Ca ratios in the foraminifera from core PC06 are typically far higher than would be expected due to temperature effects or other environmental factors (Toyofuku et al., 2000; Toler et al., 2001) it appears likely that the Mg-rich interlayers, in-filled pores and overgrowths within the foraminiferal tests from core PC06 represent authigenic precipitates. Mg abundance therefore serves as an effective tracer of the primary foraminiferal test calcite vs secondary authigenic Mg-calcite.

4.3 Contact relationship between foraminiferal calcite and authigenic carbonate overgrowths

The TEM investigation of the contacts between the original foraminiferal calcite and the authigenic Mg-calcite overgrowths was undertaken using two FIB foils milled from F1 (Fig. 5). EDX analyses confirm the compositional contrast between the calcite test and the Mg-calcite overgrowth (Fig. 5b, e-f). In addition, a sharp contact between the test and the overgrowth can be identified on high-angle annular dark-field (HAADF) images due to changes in contrast caused by differences in chemical composition (Fig. 5b-d).

Selected area electron diffractograms (SAEDs) obtained from the contact zones covering both foraminiferal tests and overgrowths (Fig. 5g-h) show that the mineral phases on both sides of the contact are structurally identical, and the crystallographic orientation is maintained though the contact. High-resolution transmission electron microscope (HRTEM) images also show that the crystal lattice fringes are identical through the contact (Fig. 5i).

The TEM data thus indicate that foraminiferal calcite serves as an ideal nucleation template for the diagenetic Mg-calcite which, despite its elevated Mg abundance, has identical structural characteristics to the foraminiferal calcite. Thus the templating capabilities of foraminifera may therefore affect the preservation of foraminifera even in environments where only minor carbonate authigenesis occurs. Although there is a wide range of carbonates in marine sediments, and several crystallographic faces are exposed, the strength of bonding at the interface is clearly strongly dependent on the structure and chemistry of the substrate surface. Our investigation demonstrates that foraminiferal calcite and authigenic Mg-calcite can have identical lattice fringes, such that authigenic Mg-calcite precipitates preferentially on foraminifera tests.

4.4 Carbon isotopic composition of primary biogenic calcite vs secondary authigenic Mg-calcite

Carbon isotope analyses on different parts of an individual test were performed on foraminifera F5 (Fig. 2). δ^{13}C values ranged from -3.9 ‰ to -34.1 ‰. Isotopically lightest carbon was found within the relatively thick Mg-calcite overgrowths, while the heaviest carbon was found within the foraminiferal calcite walls where there is only a very small amount of authigenic carbonate in-filling the test pores. It is likely that the lowest δ^{13}C values obtained from the overgrowths represent the isotopic composition of pore water DIC from which authigenic precipitates were derived. The heaviest δ^{13}C values, obtained from the foraminifera wall (-3.9 ‰), represent the carbon isotope composition closest to the original composition of the foraminiferal calcite. Given the 15µm spot size of SIMS analyses, a minor contribution from authigenic Mg-calcite in small pores (with δ^{13}C of ca. -

34 ‰) within foraminifera walls can be expected. This contribution from in-filled pores has likely caused a small shift towards more negative $\delta^{13}C$ values from the original foraminiferal calcite isotopic composition, which is not known, but is expected to be within normal marine values (ca. -1 to 1 ‰). The range of $\delta^{13}C$ values in F5 (Fig.2) is mostly due to sputtering of different proportions of the original biogenic calcite and the authigenic Mg-calcite overgrowth. The foraminiferal specimen F1, which was visually relatively well preserved, also yields relatively low $\delta^{13}C$ values of -7.7 and -11.3 ‰. This test contains abundant framboidal pyrite within its chambers, indicative of diagenetic carbon and sulfur cycling, yet there is no obvious morphologic evidence for the presence of authigenic carbonates. However, Mg/Ca mapping by EPMA reveals the presence of several Mg-rich interlayers (Fig. 4; Table 3), suggesting that cryptic authigenic Mg-calcite occurs in this test that is difficult to detect morphologically. Hence the negative $\delta^{13}C$ values of F1 also reflect the influence of methane-derived authigenic Mg-calcite on this specimen.

5. Implications

Precipitation of authigenic carbonates is expected to occur within sediments at the depth of the SMTZ at sites of methane seepage. The SMTZ can be located close to the sediment-water interface if the methane flux from depth is high, or deeper (a few cm to several tens of meters) below the interface if the methane flux is low. Thus if the methane flux is high, authigenic carbonate precipitation will be broadly coeval with the depositional age of foraminifera, and under these conditions foraminifera with authigenic overgrowths can serve as tracers of methane emission event(s) at the seafloor. On the other hand, precipitation of authigenic carbonates under low methane flux conditions can occur tens to thousands of years after sediment deposition and is likely to be decoupled from methane emissions at the seafloor. Predominance of aragonite typically reflects authigenic precipitation under high methane flux close to the sediment-water interface while Mg-calcite is associated with lower fluxes and deeper precipitation (Aloisi et al., 2000). Trace element characteristics of authigenic carbonates can also be used for deciphering between precipitation under relatively open, sea water influenced conditions close to the sediment-water interface and precipitation in subsurface sediments isolated from the overlying water column (Crémière et al., 2016a). Precipitation ages of authigenic carbonates can be determined by U-Th dating (Teichert et al., 2003; Bayon et al., 2009; Crémière et al., 2016b), although this has not yet been attempted on authigenic overgrowths on foraminifera.

Our analyses reveal the presence of authigenic carbonate overgrowths with low $\delta^{13}C$ on foraminiferal tests recovered from within sediments located both above (102 and 132 cm bsf) and below (210 cm bsf) the present-day depth of the SMTZ (184 cm bsf) in core PC06. This indicates that the depth of the SMTZ has varied over time, presumably in response to variations in methane fluxes or lateral shifts in conduit positions (e.g. Sauer et al., 2015), and the overgrowths might represent a precipitation "event" within the sediments in response to a fluctuating SMTZ. However, with our available data, we are unable to confirm whether any of the overgrowths were deposited close to the seafloor (although the presence of Mg-calcite points to precipitation below the sediment-seawater interface), and without reliable age constraints it is not possible to correlate possible methane emission and authigenic carbonate precipitation events with changes in climate parameters. For example, the authigenic overgrowths that we observe at ~200 cm bsf could have precipitated any time between the deposition of this sediment interval (> 20 000 ka; Panieri et al., 2016) and the present day.

Our findings demonstrate that foraminiferal tests incorporate methane-derived, low $\delta^{13}C$ authigenic Mg-calcite that occurs as morphologically distinct overgrowths and as cryptic pore in-fill. The ubiquitous presence of such authigenic precipitates on foraminifera in sediment records at sites of methane seepage complicates the usage of foraminifera as archives of methane emissions at the seafloor and as tracers of methane-derived DIC in the biomineralization environment because carbon isotope signatures can be modified by incorporation of light carbon at the SMTZ below the sediment-water interface. Chemical cleaning protocols to remove adhering clays, organic material and Fe-Mn oxyhydroxide phases from foraminifera have been routinely applied in trace element studies (Boyle and Keigwin, 1985; Rosenthal et al., 1999; Martin and Lea, 2002) and a weak acid leaching protocol has also been designed to chemically remove diagenetic carbonates attached to the foraminifera shell (Pena et al., 2008; Panieri et al., 2012; 2014; Consolaro et al., 2015). Isotope data obtained on such chemically cleaned foraminifera from methane seep sites can show very low δ^{13}C values (as low as -17.4 ‰ at Vestnesa Ridge) that have been interpreted to reflect the presence of methane-derived DIC in the biomineralization environment (Panieri et al., 2014). Our observations of the tight intergrown nature of biogenic calcite and authigenic Mg-calcite however draws into question the effectiveness of these cleaning procedures removing the authigenic carbonate precipitates including Mg-calcite. It is likely that authigenic carbonates, particularly the Mg-rich calcite that is notoriously difficult to remove, remain after cleaning by weak acid leaching and cause anomalous secondary ^{13}C-depletions and elevated Mg/Ca in chemically cleaned foraminifera. Moreover, these authigenic precipitates have high Mg/Ca that precludes reconstruction of past seawater temperature and thus assessment of the linkages between seafloor methane emissions and climate change. We suggest that high-resolution petrographic-elemental observations are therefore essential to ensure the authenticity of putative biogenic calcite at methane seepage sites.

Our work reveals that even foraminiferal tests that appear well-preserved under optical microscope and SEM may be diagenetically altered as a result of precipitation of authigenic phases at the depth of the SMTZ at sites of methane seepage. This potentially compromises the value of foraminiferal δ^{13}C and Mg/Ca data as records of past environmental conditions at these locations influenced by methane seepage both now and in the past. We show that fine scale analyses at sub-μm resolution allow the unaltered biogenic calcite to be targeted and thus provide the framework to overcome the challenges identified for the use of foraminifera as paleoceanographic proxies for past episodes of seafloor methane seepage and climate reconstruction.

6. Conclusions

Our work on individual tests of benthic foraminifera in a sediment core from an area of methane seepage offshore western Svalbard highlights the complexity of distinguishing between primary and secondary signals. We demonstrate that diagenetic overprints on foraminifera can be extensive, but not always evident using traditional methods such as optical microscopy. Moreover we show, for the first time, that foraminiferal calcite and authigenic Mg-calcite overgrowths have identical crystal lattice fringes, meaning they are structurally identical, such that foraminifera serve as preferred nucleation templates for authigenic Mg-calcite.

High spatial resolution analyses utilizing advanced technologies show that the authigenic Mg-calcite has much lower $\delta^{13}C$ and higher Mg/Ca than primary biogenic calcite. The low $\delta^{13}C$ values indicate the methane-derived origin of authigenic carbonate precipitating at the depth of the SMTZ. If the SMTZ is located close to the seafloor, then authigenic Mg-calcite and biogenic calcite are broadly coeval and provide a record of methane seepage at the seafloor. However, we caution that the depth of the SMTZ can be located up to several meters below the sediment-seawater interface; in these circumstances the authigenic Mg-calcite is younger than the biogenic calcite and low $\delta^{13}C$ values cannot be interpreted in terms of methane emissions at the seafloor.

ACKNOWLEDGMENTS

This work was supported by the Research Council of Norway through its Centre of Excellence funding scheme for CAGE, project number 223259, and partially supported by the UK Department of Energy and Climate Change (DECC) as part of the Natural Environment Research Council (NERC) Arctic Research Programme. We thank Trine Merete Dahl at the Department of Geology at The Arctic University of Norway in Tromsø for technical support.

FIGURE CAPTIONS

Figure 1. Location of core PC06 offshore western Svalbard in the Arctic Ocean.

Figure 2. SEM images of foraminifera F1-F5 (Table 1) from core PC06 that show different styles of diagenetic alteration. In the images of foraminifera F1 and F5, red circles and associated numbers show spots of SIMS analyses and obtained $\delta^{13}C$ values (‰ VPDB; listed in Table 2). Red squares on F1, F2, F4 and F5 indicate the areas where Mg mapping and Mg/Ca point analyses were undertaken (Fig. 3a, b, c, d respectively, and Table 3).

(a) Well preserved tests of *N. labradorica* (F1, from 132 cm bsf) exhibiting typical granular microstructure and wall pores without obvious evidence of authigenic carbonate precipitates; infilling of pyrite as framboids and small aggregates (ca. 3 μm) occurs inside the chambers (whitish areas).

(b) *N. labradorica* (F2, from 132 cm bsf;) with relatively well preserved tests exhibiting open wall pores and the systematic banding of the wall tests. White blebs are framboidal pyrite aggregates.

(c) *M. barleeanus* (F3, from 102 cm bsf). (d) Inner side of the test wall showing the foraminifera wall pores rimmed by triangular crystals of Mg-calcite. (e) Carbonate precipitation has occurred on the whole inner side of the test and the microcrystalline overgrowths completely mask the original surface features of the test. The wall pores are apparently acting as nuclei for precipitation of authigenic carbonate.

(f) *N. labradorica* (F4, from 210 cm bsf). (g) The whole inner side of the test is completely covered with microcrystalline Mg-calcite overgrowths, masking the original surface features of the test. The tops of the crystals appear as triangular prisms.

(h) *N. labradorica* (F5, from 132 cm bsf). The original part of the test (light grey areas in the backscatter image) has been covered, both on the outside and on the inside, by elongated rhombohedra crystals with sharp edges (i). SIMS data (Table 2) indicate that the secondary Mg-calcite overgrowths have low δ^{13}C values.

Figure 3. Electron backscattered images and corresponding Mg distribution maps of cross sections of *N. labradorica* and *M. barleeanus,* for images of entire foraminifera tests see Fig. 2. Red circles show locations of quantitative Mg/Ca measurements (beam diameter: ca. 2 μm) reported in Table 3.

Figure 4. Electron backscattered images and relative Mg and Ca distribution maps (middle column images where blue colors indicate low concentrations, green-red-pink colors indicate higher concentrations) from cross sections of *N. labradorica* and *M. barleeanus*, for images of entire foraminifera tests see Fig. 2. Triple images are the same place in the same individual. Red circles on the images in the first column show locations of quantitative Mg/Ca measurements (beam diameter: ca. 2 μm) reported in Table 3 and Fig. 3. The images in the last column indicate Ca maps.

Figure 5. (a) Secondary electron microscope – backscatter electron (SEM-BSE) image of a fragment of foraminifer F5 showing two locations (orange rectangles) where focused ion beam (FIB) foils, shown on panels b and d, were prepared. (b) High-angle annular dark-field (HAADF) image of entire FIB foil milled from the inner side of the foraminifera test wall. Dotted line marks the contact between foraminiferal calcite and the authigenic Mg-calcite overgrowth. Rectangles e and f give the positions of EDAX analyses shown on panels e and f. (c) HAADF close up of the contact (dotted line) between the foraminifera and authigenic overgrowth. Orange circle h gives the position of the selected area electron diffractogram (SAED) shown on panel h, and rectangle j gives the position of high-resolution transmission electron microscope (HRTEM) image shown on panel j. (d) HAADF image of entire FIB foil milled from the divider between the foraminifera chambers. Dotted line marks the contact between foraminiferal calcite and the authigenic Mg-calcite overgrowth occurring at both sides. Orange circle g gives the position of the SAED shown on panel g. (e-f) EDAX spectra

obtained from foil b showing elevated Mg content in the authigenic overgrowth compared to foraminiferal calcite where Mg is not detectable. (g-h) indexed SAED patterns from contact zones of both foils showing a consistent diffraction pattern through contacts indicating structurally identical phases with matching crystallographic orientations on both sides of contact. (i) HRTEM image from the contact zone demonstrating identical lattice fringes across the contact.

TABLE CAPTIONS

Table 1. Bulk stable carbon isotope values of foraminifera from core PC06. Data are from Panieri et al. (2016).

Table 2. Stable carbon isotope values of single foraminiferal tests (*N. labradorica*, specimen 1 and 2) analyzed with secondary ion mass spectrometry (SIMS). Values are expressed in ‰ VPDB. Locations of measurement spots are indicated in Fig. 2.

Table 3. Mg/Ca ratios measured in the inner and outer foraminiferal test walls. Locations of measurement spots are represented in Fig. 4 and indicated in the foraminiferal tests in Fig. 5.

REFERENCES CITED

Aloisi, G., Pierre C., Rouchy J.M., Foucher J.P., Woodside J., and the Medinaut Scientific Party, 2000, Methane-related authigenic carbonates of eatern Mediterranean Sea mud volcanoes and and their possible relation to gas hydrate destabilisation, Earth Planetary Science Letters, v. 184, p. 231-338.

Bayon, G., Henderson, G.M., and Bohn M., 2009, U–Th stratigraphy of a cold seep carbonate crust:

Chemical Geology, v. 260, p. 47–56, http://dx.doi.org/10.1016/j.chemgeo.2008.11.020.

Berner, R., 1970, Sedimentary pyrite formation: American Journal of Science, no. 268, p. 1-23.

Blackmon, P. D., and Todd, R., 1959, Mineralogy of some foraminifera as related to their classification and ecology: Journal of Paleontology, v. 33, p. 1–15

Boetius, A., Ravenschlag, K., Schubert, C.J., Rickert, D., Widdel, F., Giesecke, A., Amann, R., Jorgensen, B.B., Witte, U., Pfannkuche, O., 2000, A marine microbial consortium apparently mediating anaerobic oxidation of methane: Nature v. 407, p. 623– 626.

Bohaty, S.M., Zachos, J.C., and Delaney, M.L., 2012, Foraminiferal Mg/Ca evidence for Southern Ocean cooling across the Eocene–Oligocene transition: Earth Planetary Science Letters, v. 317-318, p. 251–261.

Boyle, E.A., and Rosenthal, Y., 1996, Chemical hydrography of the south Atlantic during the Last Glacial Maximum: Cd vs. δ^{13}C. In: Wefer, G., et al. (Ed.), The South Atlantic: Present and Past Circulation. Springer, New York, p. 423–443.

Branson, O., Redfern, S.A.T., Tyliszczak, T., Sadekov, A.Y., Langer, G., Kimoto, K., and Elderfield, H., 2013, The coordination of Mg in foraminiferal calcite: Earth and Planetary Science Letters, v. 383, p. 134–141.

Consolaro, C., Rasmussen, T. L. Panieri, G., Mienert, J. Buenz, S., and Sztybor, K., 2015, Carbon isotope (□13C) excursions suggest times of major methane release during the last 14 kyr in Fram Strait, the deep-water gateway to the Arctic: Climate of the Past, v. 11, p. 669–685.

Crémière, A., Lepland, A., Chand, S., Sahy, D., Kirsimäe, K., Bau, M., Whitehouse, M.J., Noble, S.R., Martma, T., Thorsnes, T. & Brunstad, H. 2016a, Fluid source and methane-related diagenetic processes recorded in cold seep carbonates from the Alvheim channel, central North Sea: Chemical Geology, v. 432, p. 6-33.

Crémière, A., Lepland, A., Chand, S., Sahy, D., Condon, D.J., Noble, S.R., Martma, T., Thorsnes, T., Sauer, S., & Brunstad, 2016b. Timescales of methane seepage on the Norwegian margin following collapse of the Scandinavian Ice Sheet. Nature Communications, in press.

de Garidel-Thoron, T.D., Rosenthal, Y., Bassinot, F., and Beaufort, L., 2005, Stable sea surface temperatures in the western Pacific warm pool over the past 1.75 million years: Nature, v. 433, p. 294-298.

Dickens, G. R., O'Neil, J. R., Rea, D. K., and Owen, R. M., 1995, Dissociation of oceanic methane hydrate as a cause of the carbon isotope excursion at the end of the Paleocene: Paleoceanography, v. 10, no. 6, p. 965–971, doi:10.1029/95PA02087.

Elderfield, H., and Ganssen G., 2000, Past temperature and δ18O of surface ocean waters inferred from foraminiferal Mg/Ca ratios: Nature, v. 405, p. 442–445.

Hesselbo, S.P., Gröcke, D.R., Jenkyns, H.C., Bjerrum, C.J., Farrimond, P., Morgans Bell, H.S., and Green, O.R., 2000, Massive dissociation of gas hydrate during a Jurassic anoxic event: Nature, v. 406, p. 392-395.

Hill, T.M., Kennett, J.P., and Valentine, D.L., 2004, Isotopic evidence for the incorporation of methane-derived carbon into foraminifera from modern methane seeps, Hydrate Ridge, Northeast Pacific: Geochimica Cosmochimica Acta, v. 68, no. 22, p. 4619–4627.

Jiang, G., Kennedy, M.J., and Christie-Blick, N., Stable isotope evidence for methane seeps in Neoproterozoic postglacial cap carbonates: Nature, v. 426, p. 822-826.

Jørgensen, B., Böttcher, M., Lüschen, H., Neretin, L., and Volkov, I., 2004, Anaerobic methane oxidation and a deep H2S sink generate isotopically heavy sulfides in Black Sea sediments: Geochimica et Cosmochimica Acta, v. 68, p. 2095-2118, doi:10.1016/j.gca.2003.07.017.

Kennett, J. P., Cannariato, K. G., Hendy, I. L., and Behl, R. J., 2000, Carbon Isotopic evidence for methane hydrate instability during Quaternary interstadials: Science, v. 288, p. 128–133.

Lea, D.W., Pak, D.K., and Spero, H.J., 2000, Climate impact of late quaternary equatorial Pacific Sea surface temperature variations: Science, v. 289, p. 1719- 1724.

Martin, P.A., Lea, D.W., 2002, A simple evaluation of cleaning procedures on fossil benthic foraminiferal Mg/Ca: Geochemistry, Geophysics, Geosystems, v. 3, no. 10, p. 8401, doi:10.1029/2001GC000280.

Martin, R. A., Nesbitt, E. A., and Campbell, K. A., 2010, The effects of anaerobic methane oxidation on benthic foraminiferal assemblages and stable isotopes on the Hikurangi Margin of eastern New Zealand: Marine Geology, v. 272, p. 270–284.

Meldrum, F.C., and Hyde, S.T., 2001, Morphological influence of magnesium and organic additives on the precipitation of calcite: Journal of Crystal Growth, v. 231, p. 544-558, ISSN 0022-0248.

Millo, C., Sarnthein, M., Erlenkeuser, H., and Frederichs, T., 2005, Methane-driven late Pleistocene δ^{13}C minima and overflow reversals in the southwestern Greenland Sea: Geology, v. 33, pp. 873–876.

Nürnberg, D., Muller, and Schneider, R., 2000, Paleo-sea surface temperature calculations in the equatorial east Atlantic from Mg/Ca ratios in planktic foraminifera: A comparison to sea surface temperature estimates from Uk37, oxygen isotopes, and foraminiferal transfer function: Paleoceanography, v. 15, p. 124-134.

Panieri, G., James, R. H., Camerlenghi, A., Westbrook, G. K., Consolaro, C., Cacho, I., Cesari, V., and Sanchez Cervera, C., 2014, Record of methane emissions from the West Svalbard continental margin during the last 23,500 years revealed by d13C of benthic foraminifera, Global Planetary Change, v. 122, p. 151–160.

Panieri, G., Graves, C.A., and James, R.H., 2016, Paleo-methane emissions recorded in foraminifera near the landward limit of the gas hydrate stability zone offshore western Svalbard: Geochemistry, Geophysics, Geosystems, v.17, p. 521–537, doi:10.1002/2015GC006153.

Peckmann, J., Gischler, E., Oschmann, W., and Reitner, J., 2001, An Early Carboniferous seep community and hydrocarbon-derived carbonates from the Harz Mountains, Germany: Geology, v. 29, p. 271–274, doi: 10.1130/0091–7613.

Rosenthal, Y., Field, M.P., and Sherrell, R.M., 1999, Precise determination of element/calcium ratios in calcareous samples using sector field Inductively Coupled Plasma Mass Spectrometry: Analytical Chemistry, v. 71, no. 15, p. 3248–3253.

Sadekov, A.Y., Eggins, S.M., and de Deckker, P., 2005, Characterization of Mg/Ca distributions in planktonic foraminifera species by electron microprobe mapping: Geochemistry, Geophysics, Geosystems, v. 6, Q12P06.

Teichert B.M.A., Eisenhauer A., Bohrmann, G. Haase-Schramm, A. Bock B., and Linke, P., 2003, U/Th systematics and ages of authigenic carbonates from Hydrate Ridge, Cascadia Margin: recorders of fluid flow variations: Geochimica Cosmochimica Acta, v. 67, p. 3845–3857, http://dx.doi.org/10.1016/S0016-7037(03)00128-5.

Toyofuku, T., Kitazato, H., Kawahata, H., Tsuchiya, M., and Nohara, M., 2000, Evaluation of Mg/Ca thermometry in foraminifera: Comparison of experimental results and measurements in nature: Paleoceanography, v. 15, p. 456–464.

Toler, S. K., Hallock, P., and Schijf, J., 2001, Mg/Ca ratios in stressed foraminifera, Amphistegina gibbosa, from the Florida Keys: Marine Micropaleontology, v. 43, p. 199–206.

Torres, M. E., Martin, R. A., Klinkhammer, G. P., and Nesbitt E. A., 2010, Post depositional alteration of foraminiferal shells in cold seep settings: New insights from flow-through time-resolved analyses of biogenic and inorganic seep carbonates: Earth and Planetary Science Letters, v. 299, p.10–22.

Ussler III, W., and Paull, C. K., 2008, Rates of anaerobic oxidation of methane and authigenic carbonate mineralization in methane-rich deep-sea sediments inferred from models and geochemical profiles: Earth and Planetary Science Letters, v. 266, p. 271-287, doi:10.1016/j.epsl.2007.10.056.

Walter, L.M., 1986. Relative efficiency of carbonate dissolution and precipita- tion during diagenesis: a progress report on the role of solution chemistry. In Gautier, D.L. (Ed.), Roles of Organic Matter in Sediment Diagenesis. The Society of Economic Paleontologists and Mineralogists Special Publication, v. 38, pp. 1–11.

Wefer, G., Heinze, P.-M., and Berger, W. H., 1994, Clues to ancient methane release: Nature, v. 369, p. 282, 1994.

Wirth, R., 2009, Focused Ion Beam (FIB) combined with SEM and TEM: Advanced analytical tools for studies of chemical composition, microstructure and crystal structure in geomaterials on a nanometre scale: Chemical Geology, v. 261, no. 3-4, p. 217—229, doi: http://doi.org/10.1016/j.chemgeo.2008.05.019

Wright, D.T., and Wacey, D., 2004, Sedimentary dolomite - a reality check. The Geometry and Petrogenesis of Dolomite Hydrocarbon Reservoirs: Geological Society, London, Special Publication v. 235, p. 65-74.

Zachos, J.C., Rhöl, U., Schellenberg, S.A., Sluijs, A., Hodell, D.A., Kelly, D.C., Thomas, E., Nicolo, M., Raffi, I., Lourens, L.J., McCarren, H., and Kroon, D., 2005. Rapid acidification of the ocean during the Paleocene-Eocene thermal maximum: Science, v. 308, p. 1611-1615, doi:10.1126/science.1109004

[1]GSA Data Repository item 201Xxxx, The data are stored at the Centre for Arctic Gas Hydrate, Environment and Climate data repository and are accessible by contacting fabio.sarti@uit.no., is available online at www.geosociety.org/pubs/ft20XX.htm, or on request

Figure 1

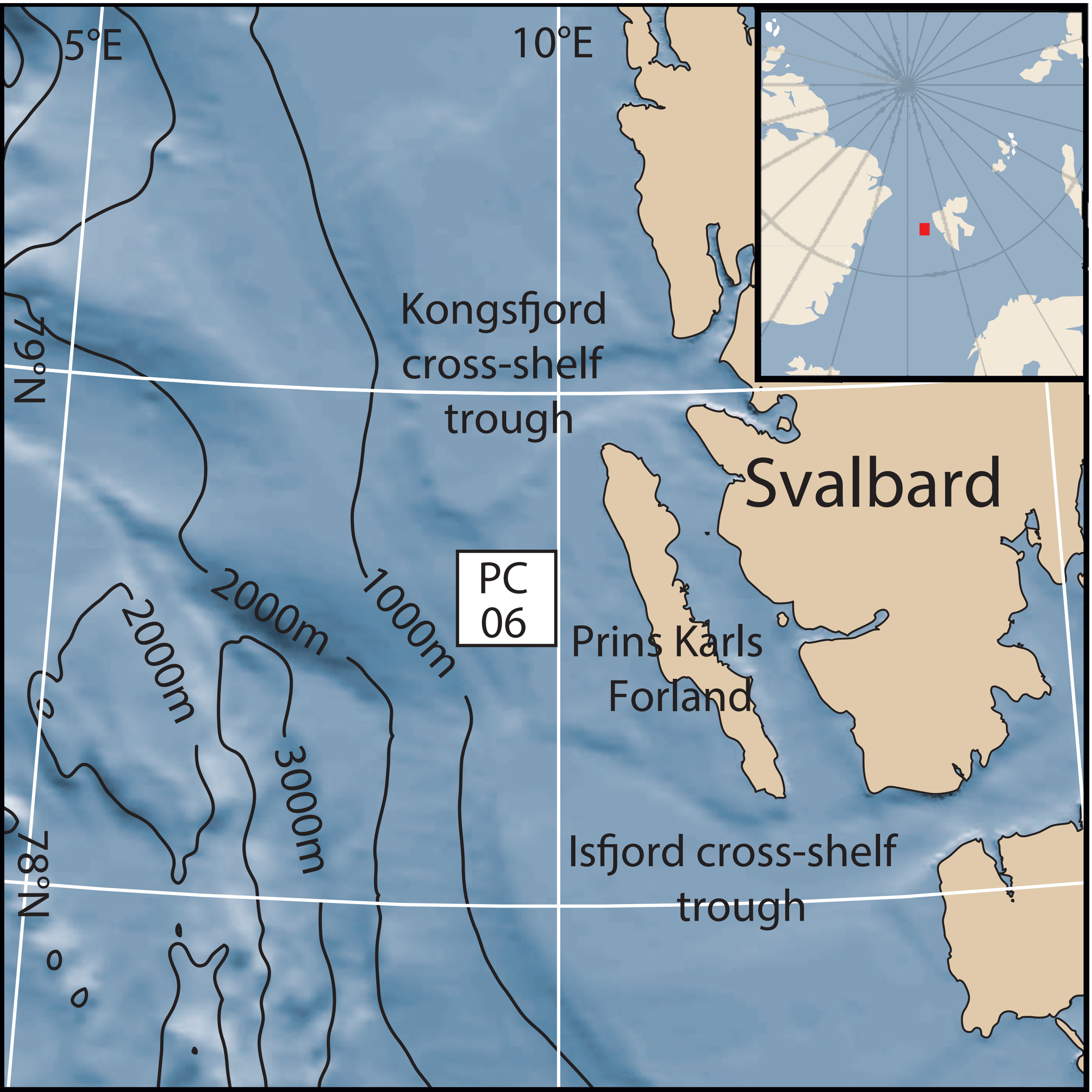
5°E
10°E
79°N
78°N
Kongsfjord cross-shelf trough
Svalbard
PC 06
Prins Karls Forland
Isfjord cross-shelf trough
2000m
2000m
1000m
3000m

Figure 2

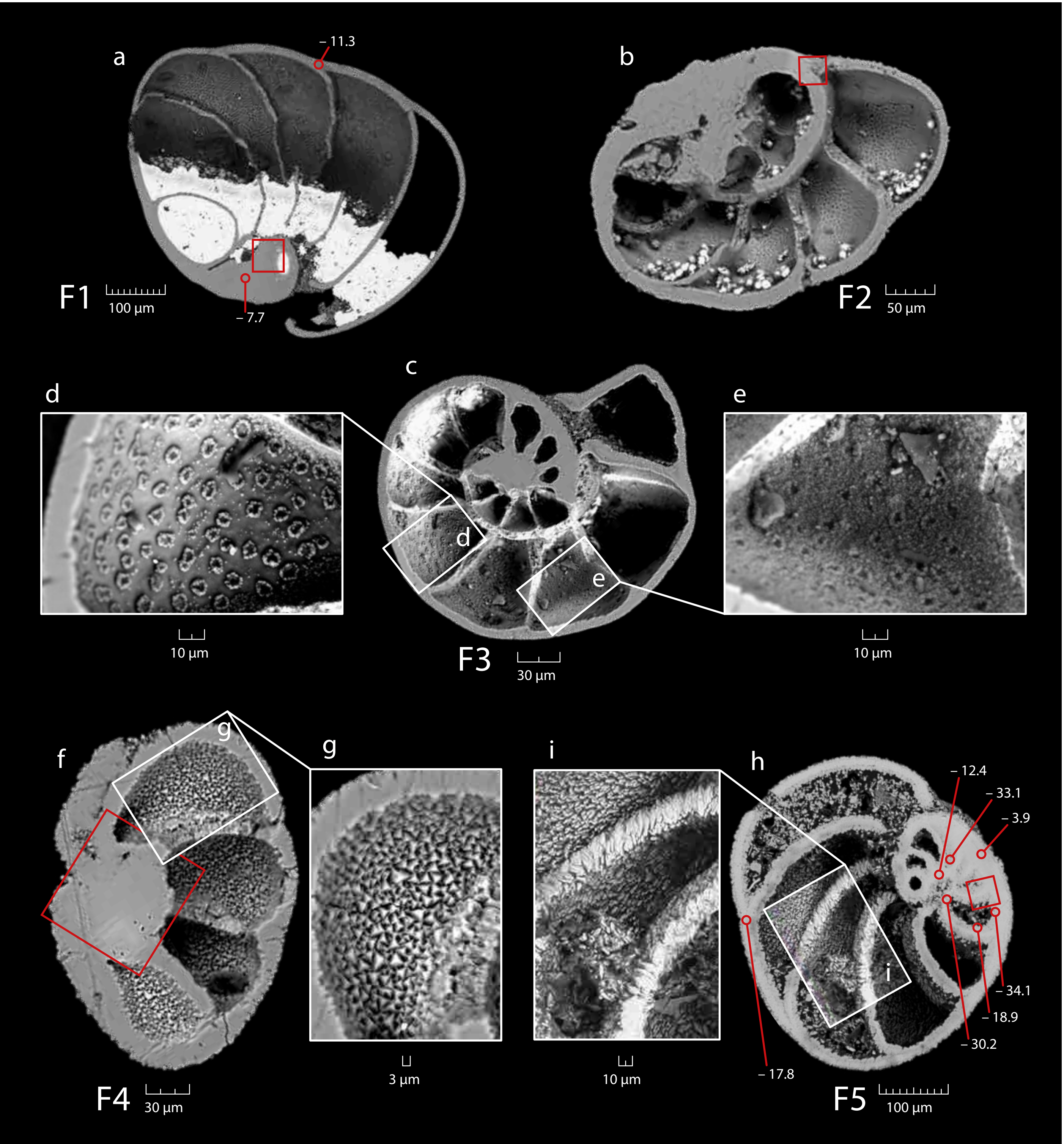
a
– 11.3
– 7.7
F1
100 µm
b
F2
50 µm
c
d
e
d
10 µm
F3
30 µm
e
10 µm
f
g
g
3 µm
F4
30 µm
i
10 µm
h
– 12.4
– 33.1
– 3.9
i
– 34.1
– 18.9
– 30.2
– 17.8
F5
100 µm

Figure 3

Click here to download high resolution image

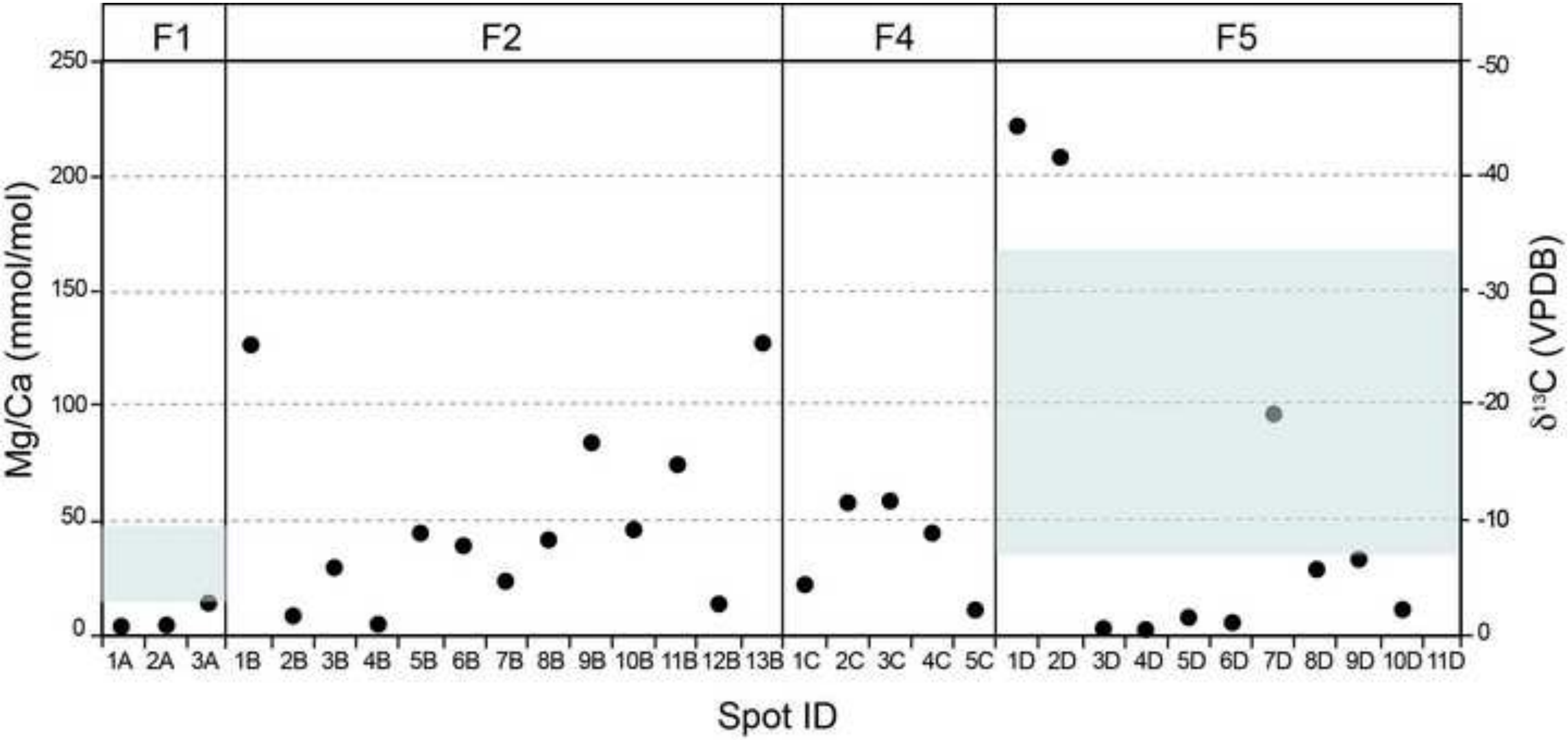

Figure 4

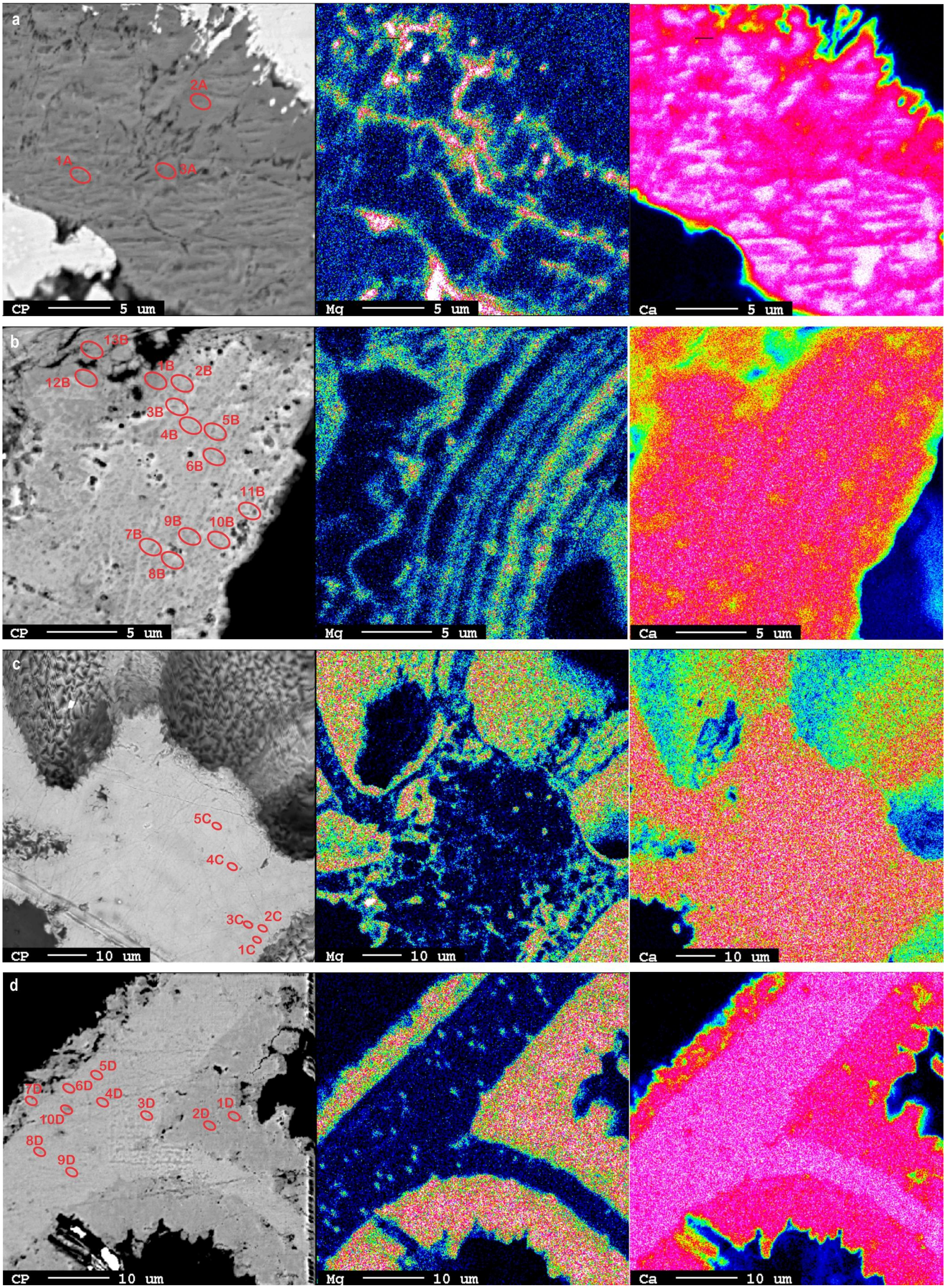
a
2A
1A
3A
CP 5 um
Mg 5 um
Ca 5 um
b
13B
12B
1B
2B
3B
4B
5B
6B
11B
9B
10B
7B
8B
CP 5 um
Mg 5 um
Ca 5 um
c
5C
4C
3C
2C
1C
CP 10 um
Mg 10 um
Ca 10 um
d
5D
6D
7D
4D
3D
1D
2D
10D
8D
9D
CP 10 um
Mg 10 um
Ca 10 um

Figure 5

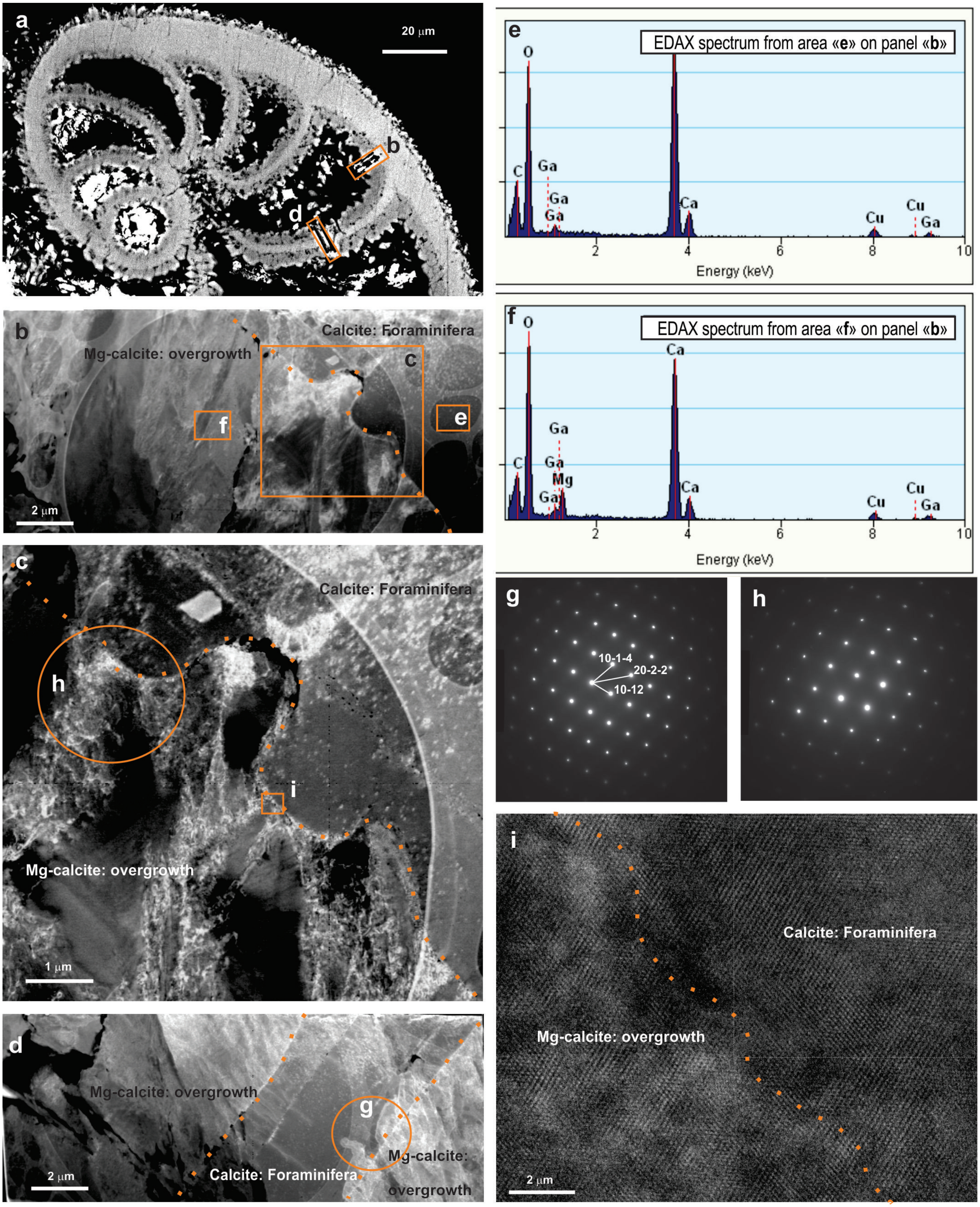
a
20 µm
b
d
b
Calcite: Foraminifera
Mg-calcite: overgrowth
c
f
e
2 µm
c
Calcite: Foraminifera
h
i
Mg-calcite: overgrowth
1 µm
d
Mg-calcite: overgrowth
g
Calcite: Foraminifera
Mg-calcite: overgrowth
2 µm
e
EDAX spectrum from area «e» on panel «b»
O
C
Ga
Ga
Ga
Ca
Cu
Cu
Ga
2
4
6
8
10
Energy (keV)
f
EDAX spectrum from area «f» on panel «b»
O
Ca
Ga
C
Ga
Mg
Ga
Ca
Cu
Cu
Ga
2
4
6
8
10
Energy (keV)
g
10-1-4
20-2-2
10-12
h
i
Calcite: Foraminifera
Mg-calcite: overgrowth
2 µm

Table 1-3

Foraminifera	Species	Depth (cm bsf)	$\delta^{13}C$
F1	*Nonionella labradorica* (specimen 2)	132	-10.6
F2	*Nonionella labradorica*	102	-4.7
F3	*Melonis barleenaum*	102	-5.1
F4	*Nonionella labradorica*	210	-11.3
F5	*Nonionella labradorica* (specimen 1)	132	-10.6